7-15-2022

Reducing leakage current and enhancing polarization in multiferroic 3D supernanocomposites by microstructure engineering

Erik Enriquez

Ping Lu

Leigang Li

Bruce Zhang

Haiyan Wang

See next page for additional authors

Authors
Erik Enriquez, Ping Lu, Leigang Li, Bruce Zhang, Haiyan Wang, Quanxi Jia, and Aiping Chen

Reducing leakage current and enhancing polarization in multiferroic 3D super-nanocomposites by microstructure engineering

OPEN ACCESS
IOP Publishing
Nanotechnology

Nanotechnology **33** (2022) 405604 (7pp)
https://doi.org/10.1088/1361-6528/ac5f98

Reducing leakage current and enhancing polarization in multiferroic 3D super-nanocomposites by microstructure engineering

Erik Enriquez[1,*], Ping Lu[2], Leigang Li[3], Bruce Zhang[3], Haiyan Wang[3], Quanxi Jia[4,5] and Aiping Chen[6,*]

[1] Department of Physics and Astronomy, University of Texas—Rio Grande Valley (UTRGV), Edinburg, TX-78539, United States of America
[2] Sandia National Laboratories, Albuquerque, New Mexico NM-87185, United States of America
[3] School of Materials Engineering, Purdue University, West Lafayette, Indiana IN-47907, United States of America
[4] Department of Materials Design and Innovation, University at Buffalo - The State University of New York, Buffalo, NY-14260, United States of America
[5] Division of Quantum Phases & Devices, Department of Physics, Konkuk University, Seoul 05029, Republic of Korea
[6] Center for Integrated Nanotechnology (CINT), Los Alamos National Laboratory, Los Alamos, NM-87545, United States of America

E-mail: erik.enriquez01@utrgv.edu and apchen@lanl.gov

Received 16 December 2021, revised 8 March 2022
Accepted for publication 21 March 2022
Published 15 July 2022

Abstract

Multiferroic materials have generated great interest due to their potential as functional device materials. Nanocomposites have been increasingly used to design and generate new functionalities by pairing dissimilar ferroic materials, though the combination often introduces new complexity and challenges unforeseeable in single-phase counterparts. The recently developed approaches to fabricate 3D super-nanocomposites (3D-sNC) open new avenues to control and enhance functional properties. In this work, we develop a new 3D-sNC with $CoFe_2O_4$ (CFO) short nanopillar arrays embedded in $BaTiO_3$ (BTO) film matrix via microstructure engineering by alternatively depositing BTO:CFO vertically-aligned nanocomposite layers and single-phase BTO layers. This microstructure engineering method allows encapsulating the relative conducting CFO phase by the insulating BTO phase, which suppress the leakage current and enhance the polarization. Our results demonstrate that microstructure engineering in 3D-sNC offers a new bottom–up method of fabricating advanced nanostructures with a wide range of possible configurations for applications where the functional properties need to be systematically modified.

Keywords: nanocomposites, epitaxial growth, microstructure

(Some figures may appear in colour only in the online journal)

* Authors to whom any correspondence should be addressed.

In order to optimize and enhance material properties, there is a strong need to design material structure at the nanoscale. Recent research in vertically aligned nanocomposite (VAN) thin films has demonstrated that multifunctionalities can be integrated and tuned at the vertical interface [1]. VAN structure provides a variety of approaches to control microstructure and strain at the nanoscale, which could enable functions by design [2, 3]. VAN has become a platform to host different types of materials with various functional properties. Particularly, multiferroic VANs by integrating ferroelectric and ferromagnetic components have attracted great attention in the past decade [4–10]. One of the challenges of multiferroic VANs is that the ferromagnetic pillar phase, often penetrating through the whole film, is relatively conductive. With the exception of reducing the leakage current by incorporating different materials, microstructure engineering at nanoscale could be an effective approach to solve this issue.

Recent developments in synthesizing 3D super-nanocomposites (3D-sNC) have attracted much attention [11]. By integrating VAN with multilayer structure, 3D-sNC with different designs and geometries have been enabled and are capable of synthesizing more advanced nanostructures [12]. The microstructure engineering in 3D-sNc has been used to tune magneto transport and magnetic properties [13–15]. Li *et al* designed $BiFeO_3$:$CoFe_2O_4$ nanocomposites with $CoFe_2O_4$ nanoparticle arrays in $BiFeO_3$ matrix where the enhanced magnetoelectric coupling could be achieved due partially to the reduced leakage current [16]. Therefore, the 3D-sNC structure could be an ideal structure to enable magnetoelectric nanocomposites. However, the effect of the microstructure design on leakage current and polarization in such 3D-sNC is not clear. Here, we report on the effects of BTO geometry on the electronic conductivity and polarization properties in $BaTiO_3$ (BTO):$CoFe_2O_4$ (CFO) 3D-sNC thin films. By tuning the BTO interlayer thickness and composition, the leakage current and polarization of the system can be tuned. Our work provides insight into microstructure engineering to control functional properties in multiferroic nanocomposite thin films. Beyond our results, this research suggests a wide range of possible implementations by selecting appropriate materials combination and architectural design to further tune functionalities.

Epitaxial BTO:CFO 3D-sNC thin films were grown on $SrRuO_3$ buffered $SrTiO_3$ (001) substrates by pulsed laser deposition using a KrF excimer laser (Lambda Physik LPX 305, $\lambda = 248$ nm, 4 Hz). The BTO:CFO composite target used for the deposition was fabricated by a conventional ceramic sintering process with a molar ratio of 50% $BaTiO_3$/50% $CoFe_2O_4$. The 3D-sNC thin films were grown by alternatively depositing BTO:CFO VAN layers and BTO single-phase layers. A rectangle laser beam was focused onto the target with an optimized energy density of 2.0 J cm^{-2} for film growth. Prior to the deposition, the chamber was pumped down to a base pressure of 5×10^{-7} Torr. A substrate temperature of 750 °C was maintained during all depositions. An optimized growth pressure of 200 mTorr for BTO and 50 mTorr for BTO:CFO was used during film growth. Both the target and the substrate are rotated during the deposition to achieve better uniformity. After deposition, the chamber was filled with 500 Torr ultra-high purity O_2. The samples were held at 750 °C for 15 min, followed by cooling at 5 °C min^{-1} to 25 °C.

X-ray diffraction (Panalytical X'Pert PRO MRD), both 2θ-ω and reciprocal space mapping (RSM), was employed to obtain information on the orientation, lattice parameters and epitaxial quality of the thin films. Scanning transmission electron microscopy (STEM) was used to investigate the film microstructure. A FEI Titan^{TM} G2 80–200 STEM with a Cs probe corrector and ChemiSTEM^{TM} technology (X-FEG^{TM} and SuperX^{TM} energy-dispersive x-ray spectroscopy (EDS) with four windowless silicon drift detectors) operated at 200 kV was used in this study. EDS and high-angle annular dark-field (HAADF) imaging were used for compositional and structural analysis, respectively. The EDS spectral imaging was acquired as a series of frames, where the same region was scanned multiple times. EDS spectral imaging was analyzed by multivariate analysis using the principal component analysis (PCA) method [17]. Leakage current of the materials was characterized at room temperature by Agilent E4980A Precision LCR meter and polarization was measured by Precision LC analyzer (Radiant Technologies). Circular Au top electrodes of 350 μm in diameter defined by a shallow mask were grown by sputtering.

$(BTO/BTO:CFO)_n/BTO$ heterostructures were grown on $SrRuO_3$ (SRO, 25 nm) bottom electrodes on $SrTiO_3$ substrates with varying interlayer BTO thicknesses and periodicity (n =2, 3), where both sample configurations are shown in figure 1(a). $(BTO/BTO:CFO)_2/BTO$ samples with two BTO:CFO layers enclosed in three BTO interlayers (i.e. BTO/BTO:CFO/BTO/BTO:CFO/BTO) are labeled BTO_{3B}. $(BTO/BTO:CFO)_3/BTO$ samples with three BTO:CFO layers enclosed by four BTO interlayers are labeled as BTO_{4B}. XRD results for all BTO_{3B} samples of varying BTO interlayer thickness and a control sample of BTO:CFO without BTO interlayer insertion are shown in figure 1(b). In the BTO:CFO sample, a clear peak can be distinguished for SRO and CFO phases, but the BTO peak is mostly overlapped with the CFO signal. This peak becomes more distinguished by the increase in thickness of the BTO interlayer in the 15 nm BTO_{3B} and 30 nm BTO_{3B} samples. 15 nm BTO_{3B} sample has a BTO interlayer thickness of 15 nm. The BTO peak shifts to higher angles and the out-of-plane lattice parameter decreases from 4.06 to 4.02 Å with increasing BTO thickness. The CFO peak shifts slightly toward higher angle with increasing BTO interlayer thickness. It is known that there is a large lattice mismatch of 3.71% between BTO and CFO phases. In BTO:CFO VAN, BTO will be in tension and CFO will be in compression out-of-plane [6]. This agrees with the results obtained by XRD, which suggests that the CFO out-of-plane lattice parameter is approximately 8.12 Å. This is equivalent to an approximate compressive strain of ~3.1% in the CFO

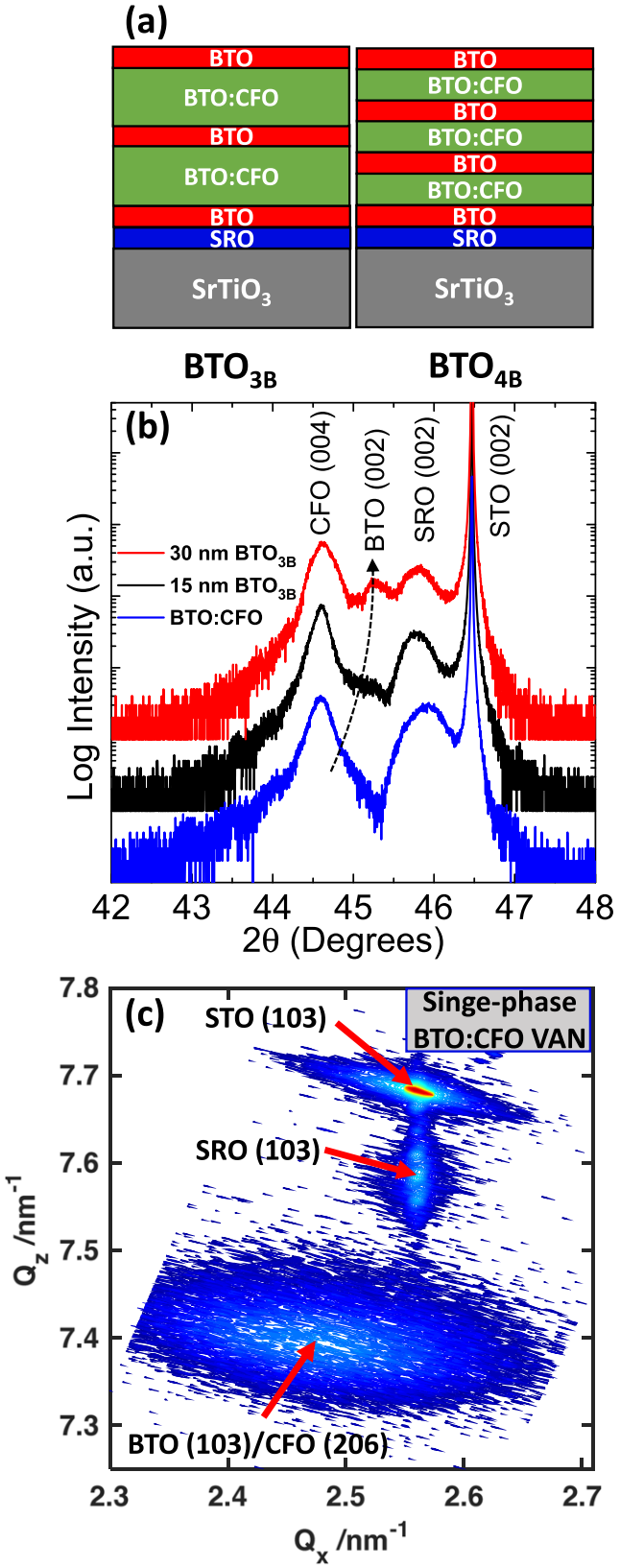

Figure 1. (a) Illustration of BTO_{3B} and BTO_{4B} VAN heterostructures. (b) 2θ-ω XRD scan of BTO:CFO, 15 nm BTO_{3B} and 30 nm BTO_{3B} samples. 15 nm BTO_{3B} means 2 layers of BTO:CFO VANs are separated by 3 layers BTO with 15 nm of each BTO layer. (c) RSM of a BTO:CFO VAN near STO (103) peak.

phase relative to a bulk value of 8.38 Å. RSM results are presented in figure 1(c). The small nanopillar size and large interfacial area between these two VAN phases are the main reasons for the high strain coupling [5].

Figures 2(a) and (b) show cross-sectional STEM HAADF images along with EDS of 15 nm BTO_{4B} and 30 nm BTO_{3B} samples, respectively. The EDS results confirm the targeted thickness and delineation of BTO and BTO:CFO layers. The nanocomposite phase shows a meandering CFO pillar structure, which is expected for BTO:CFO VAN films of this thickness and composition. The interfacial structure is presented in figures 2(c) and (d). The clear phase separation of the *c*-axis oriented BTO and CFO phases can be identified. The CFO has lattice parameters $a = c = 8.38$ Å in bulk, which can match the BTO lattice ($a = 3.99$ Å, $c = 4.04$ Å in bulk) with approximately half the size of CFO unit cell.

The incorporation of BTO interlayers in BTO:CFO VAN plays a critical role in electronic transport properties. While BTO:CFO is an intriguing architecture that combines ferroelectric and ferromagnetic properties to generate a multiferroic bulk property, there is an added complexity when combining phases in a VAN thin film. Even when combining two insulating phases, interfacial conduction between the phases can dominate the overall electronic properties [18–20]. In the case of BTO and CFO, the ferrimagnetic CFO phase is more conductive and can introduce a conduction path through the VAN film. The BTO interlayers create a discontinuity in the conduction pathways through CFO and BTO:CFO interface, as illustrated in figure 3(a). *I*–*V* characteristics of the BTO:CFO samples with and without BTO interlayers were measured, with the results and analysis shown in figures 3(b)–(d). A clear reduction of leakage current was observed, where increasing thickness of BTO interlayers decreased the conductivity of the heterostructure up to a field of 86.2 MV m^{-1}. Similar conductivity behavior was observed for 15 nm BTO_{4B} and 30 nm BTO_{3B}, which have interlayers that occupy a similar volume of the total heterostructures, at 27% and 31%, respectively. This suggests that in the range of interlayer thicknesses investigated, the total BTO interlayer volume is more efficient to reduce leakage current than the number of interlayers, which is consistent with the results summarized in figure 3(d). The lowest leakage current achieved in the sample with the 45 nm BTO_{3B} is ~17.2 A m^{-2} at 86.2 MV m^{-1}. This is a reduction of 96.8% in leakage current when compared to pure BTO:CFO VAN structure. This result is consistent with the equivalent circuits for BTO:CFO and 3D nanocomposites as shown in figure 3(a). In 3D-sNC, the BTO interlayers provides series resistance and capacitance which significantly reduce the leakage current compared to BTO:CFO without interlayers. It is reasonable to assume that leakage current could be decreased and the ferroelectric properties will be improved by further increasing volume of the BTO phase. In addition, to optimizing the multiferroic properties, there should be a suitable phase ratio. Early work has theoretically predicted volume dependent magnetoelectric couplings in

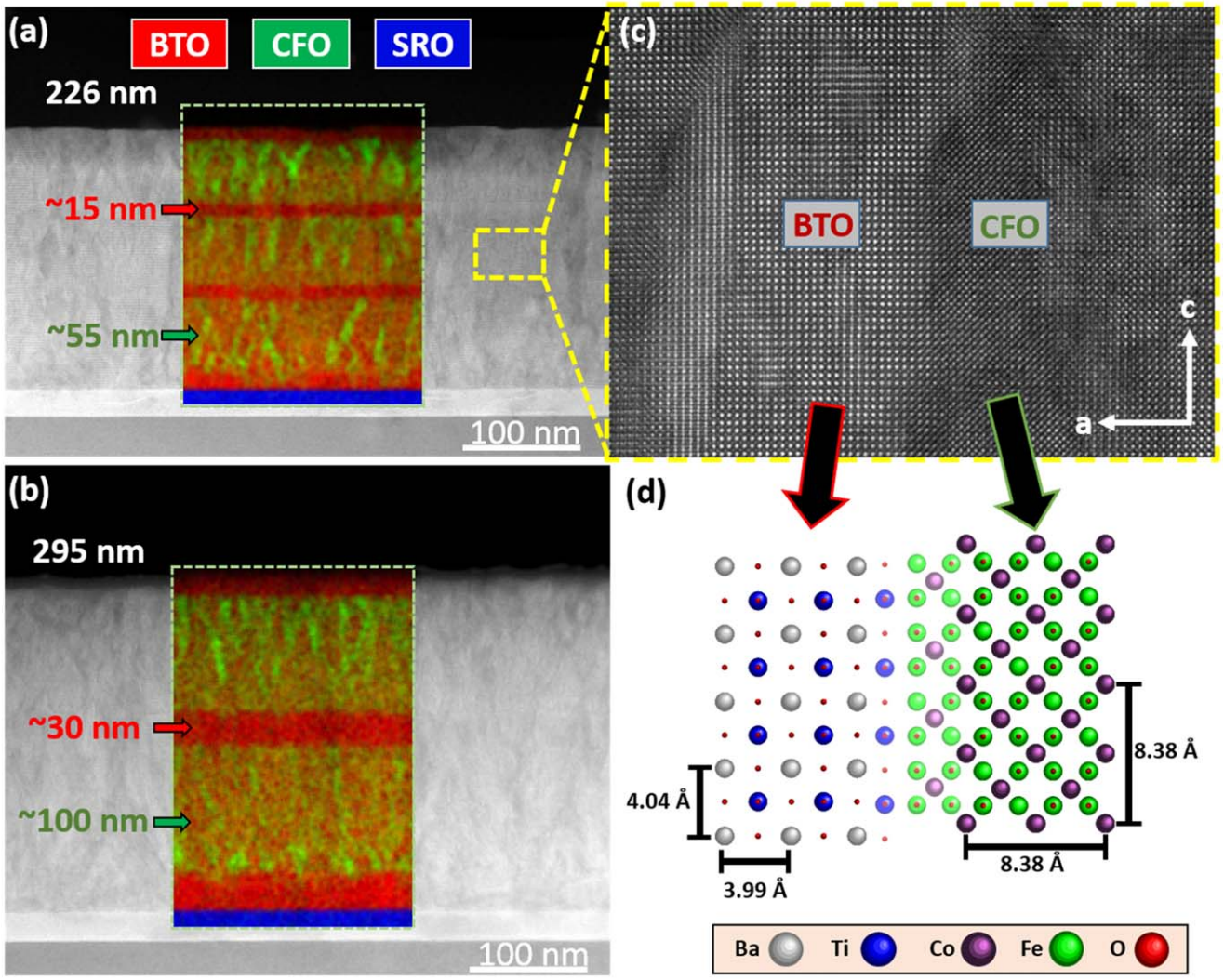

Figure 2. STEM cross-section images of (a) 15 nm BTO_{4B} and (b) 30 nm BTO_{3B} samples with EDS insets showing maps obtained by the PCA analysis: BTO (red), CFO (green), and SRO (blue) phases. (c) High-resolution STEM image of BTO/CFO interface. (d) Illustration of BTO and CFO lattice structures with bulk lattice parameter values and interfacial region.

vertical nanocomposites and multilayers [21]. But such a prediction in 3D nanocomposites is rare. Optimization of BTO and CFO volume ratio will need further study. Table 1 provides a summary of the sample details and electronic properties of the samples at a field of 86.2 MV m^{-1}.

Electric polarization hysteresis curves for all samples are shown in figure 4. Due to the larger leakage current, BTO:CFO VANs show a *P-E* loop in a banana shape. This is due to the relatively conducting CFO pillars penetrating through the VANs. The obtained polarization ~40 μC cm^{-2} can be misleading due to the large leakage current. The 3D-sNC can be an effective approach to solve this problem by encapsulating CFO pillars by insulating BTO matrix. The incorporation of the thinnest BTO interlayers, 15 nm BTO_{3B}, occupying 16% of the total heterostructure volume, suppresses the leakage current and a well-defined *P-E* loop is seen. Interestingly, increasing the interlayer thickness and/or total volume clearly shows the increase in magnitude of the polarization. The maximum polarization value of the 45 nm BTO_{3B} sample at 86.2 MV m^{-1} was measured to be approximately 30 μC cm^{-2}, which is close to pure BTO thin films [22]. But the remanent polarization is ~10 μC cm^{-2}, which is less than single phase films (~20 μC cm^{-2}). Both the ferroelectric performance and leakage current density must be taken into account from a functional property standpoint. Further work is needed to improve the remanent polarization for memory device applications. For example, the volume ratio of BTO can be further optimized to tune the ferroelectric response. BTO is a promising lead-free ferroelectric material for electronic device applications [23]. Since the incorporation of BTO interlayers can reduce the leakage current significantly, such a nanocomposite can be used to synthesize BTO:CFO VANs for multiferroic applications. In addition, although the interlayer

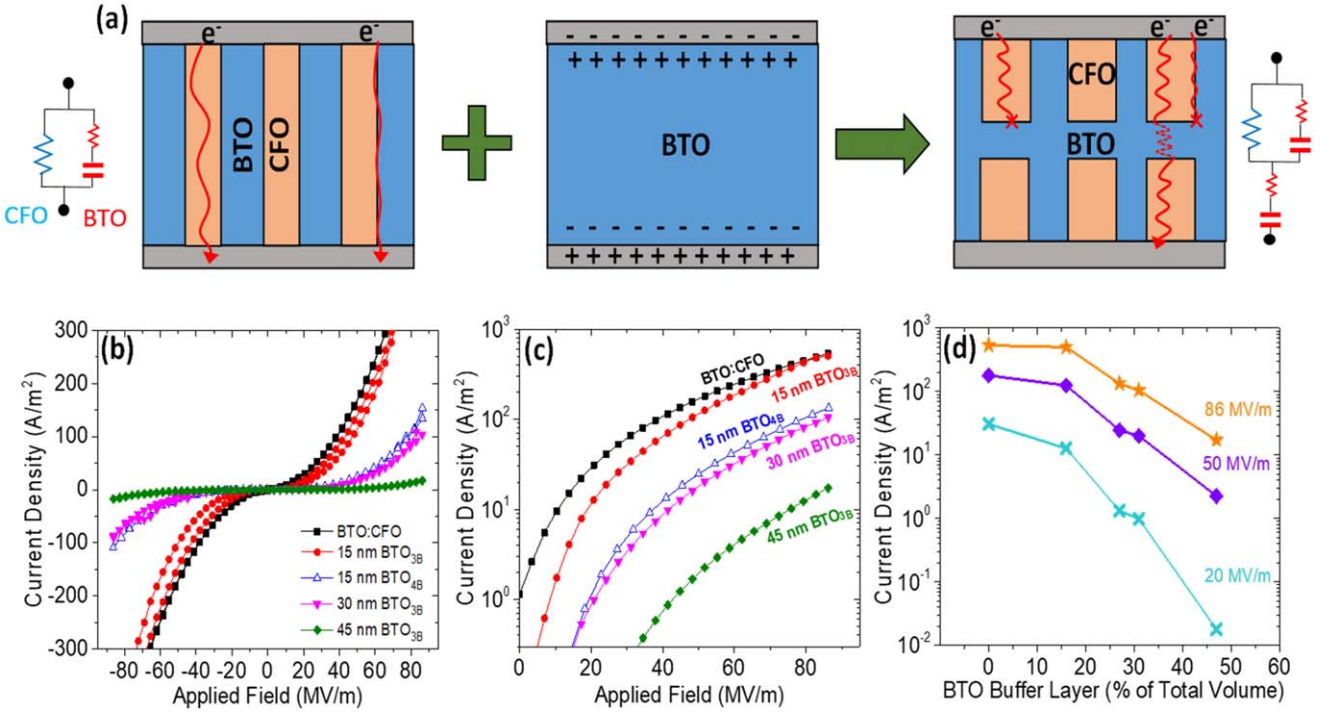

Figure 3. (a) Conceptual illustration of nanocomposite BTO:CFO which has multiferroic properties but creates conduction path that can degrade device performance. The BTO interlayers can act as a barrier to reduce the conduction. Red lines show examples of possible paths of conduction at the BTO:CFO interface and within the CFO pillars. Illustrations on the left and right show the equivalent circuits for BTO:CFO and 3D nanocomposites. (b) *I–V* characteristics of BTO_{3B} and BTO_{4B} samples compared to BTO:CFO. (c) Log scale of the *I–V* characteristics under forward bias with different BTO interlayer thickness. (d) Leakage current density versus BTO interlayer volume % of total heterostructures for all samples.

Table 1. Summary of film thickness, volume ratios, and select electrical characterization data for BTO:CFO with BTO interlayer heterostructures. Current density was at 86.2 MV m^{-1}.

	Total thickness (nm) (BTO/BTO:CFO)	BTO buffer layer volume ratio	Current density (mA cm^{-2})	Maximum polarization ($\mu C\ cm^{-2}$)
BTO:CFO	285 (0/285)	0% BTO	53.447	—
15 nm BTO_{3B}	285 (45/240)	16% BTO	50.255	∼20
15 nm BTO_{4B}	225 (60/165)	27% BTO	13.345	∼25
30 nm BTO_{3B}	290 (90/200)	31% BTO	10.433	∼25
45 nm BTO_{3B}	285 (135/150)	47% BTO	1.722	∼30

chosen
for this application was BTO in part for its structural simplicity when incorporated with BTO:CFO, other interlayer materials can be used in other applications with varying active roles, such as to improve chemical and structural compatibility with substrate materials [24], tuning magnetic/electronic properties [25, 26], epitaxial orientation control [27], diffusion barriers [28], and increasing the Curie temperature [29, 30], among many others. This extends the possibilities afforded by the incorporation of interlayers which could strike a balance between VAN multiferroic properties and functionalities generated by proper selection and architecture of an interlayer/VAN heterostructure. Our results show the potential of another nanoarchitectural avenue in the expansive study of thin film materials with designable physical properties.

To summarize, this research demonstrates a method of controlling the current conduction behavior in multiferroic BTO:CFO 3D-sNC thin films via tuning the microstructure and geometry. The presence of interlayers can significantly reduce the leakage current. Polarization of the overall assembly can be tuned in the 3D-sNC heterostructures when compared to a simple VAN BTO:CFO, but also shows strong dependence on interlayer thickness. Using 3D-sNC with appropriate interlayer materials, the multifunctional properties of a VAN thin film can be further improved. Beyond the

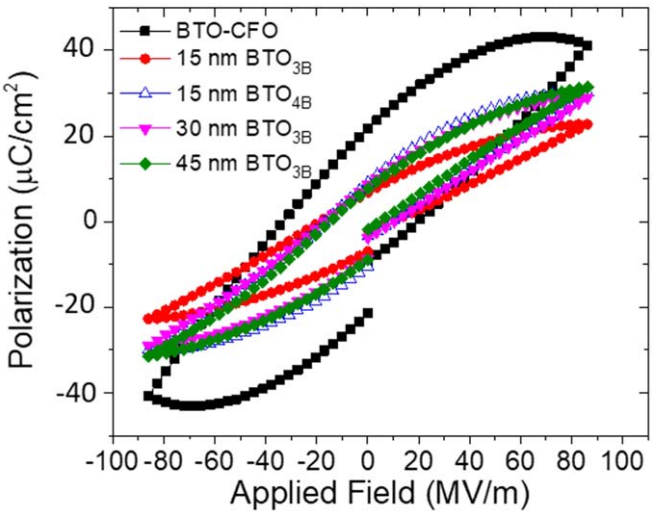

Figure 4. Polarization-electric field hysteresis loop showing ferroelectric property of BTO:CFO VANs and 3D super-nanocomposite samples.

results demonstrated here, this method can be adapted to fit a wide range of possible configurations and applications to modify or enhance functional properties in vertically-aligned nanocomposite thin film structures.

Acknowledgments

The work at Los Alamos National Laboratory was supported by the NNSA's Laboratory Directed Research and Development Program and was performed, in part, at the Center for Integrated Nanotechnologies (CINT), an office of Science User Facility operated for the U.S. Department of Energy Office of Science. Los Alamos National Laboratory, an affirmative action equal opportunity employer, is managed by Triad National Security, LLC for the U.S. Department of Energy's NNSA, under contract 89233218CNA000001. The effort at University at Buffalo was supported by the US. National Science Foundation, ECCS-1902623. Q. X. Jia acknowledges the support from the CINT Users Program. Sandia National Laboratories is a multiprogram laboratory managed and operated by National Technology and Engineering Solutions of Sandia, LLC, a wholly owned subsidiary of Honeywell International, Inc., for the U.S. Department of Energy's National Nuclear Security Administration under contract DE-NA0003525. This paper describes objective technical results and analysis. Any subjective views or opinions that might be expressed in the paper do not necessarily represent the views of the U.S. Department of Energy or the United States Government.

Data availability statement

All data that support the findings of this study are included within the article (and any supplementary files).

Conflict of interest

The authors have no known conflict of interests concerning the publication of this research.

ORCID iDs

Haiyan Wang https://orcid.org/0000-0002-7397-1209
Quanxi Jia https://orcid.org/0000-0002-7683-5202
Aiping Chen https://orcid.org/0000-0003-2639-2797

References

[1] Chen A P, Su Q, Han H, Enriquez E and Jia Q X 2019 *Adv. Mater.* **31** 1803241
[2] Huang J, MacManus Driscoll J L and Wang H Y 2017 *J. Mater. Res.* **32** 4054
[3] MaCmanus-Driscoll J L, Zerrer P, Wang H Y, Yang H, Yoon J, Fouchet A, Yu R, Blamire M G and Jia Q X 2008 *Nat. Mater.* **7** 314
[4] Stratulat S M, Lu X L, Morelli A, Hesse D, Erfurth W and Alexe M 2013 *Nano Lett.* **13** 3884
[5] Zheng H *et al Science* **303** 6612004
[6] Chen A P *et al Adv. Sci.* **6** 19010002019
[7] Dix N, Muralidharan R, Guyonnet J, Warot-Fonrose B, Varela M, Paruch P, Sanchez F and Fontcuberta J 2009 *Appl. Phys. Lett.* **95** 062907
[8] Wang Z G, Yang Y D, Viswan R, Li J F and Viehland D 2011 *Appl. Phys. Lett.* **99** 043110
[9] Oh Y S, Crane S, Zheng H, Chu Y H, Ramesh R and Kim K H 2010 *Appl. Phys. Lett.* **97** 052902
[10] Schmitz-Antoniak C *et al* 2013 *Nat. Commun.* **4** 2051
[11] Chen A P and Jia Q X 2021 *MRS Bull.* **46** 115
[12] Chen A P *et al* 2019 *Adv. Funct. Mater.* **29** 1900442
[13] Kim D H, Aimon N M, Sun X Y and Ross C A 2014 *Adv. Funct. Mater.* **24** 2334
[14] Ning X K, Wang Z J and Zhang Z D 2014 *Adv. Funct. Mater.* **24** 5393
[15] Sun X, Li Q, Huang J, Fan M, Rutherford B X, Paldi R L, Jian J, Zhang X and Wang H 2019 *Appl. Mater. Today.* **16** 204
[16] Li Y X *et al* 2015 *Nat. Commun.* **6** 6680
[17] Kotula P G, Keenan M R and Michael J R 2003 *Microsc. Microanal.* **9** 1
[18] Bark C, Sharma P, Wang Y, Baek S H, Lee S, Ryu S, Folkman C, Paudel T R, Kumar A and Kalinin S V 2012 *Nano Lett.* **12** 1765
[19] Li W W, Zhao R, Tang R J, Chen A P, Zhang W R, Lu X, Wang H Y and Yang H 2014 *ACS Appl. Mater. Interfaces* **6** 5356
[20] Hsieh Y H, Liou J M, Huang B C, Liang C W, He Q, Zhan Q, Chiu Y P, Chen Y C and Chu Y H 2012 *Adv. Mater.* **24** 4564
[21] Liu G, Nan C-W, Xu Z and Chen H 2005 *J. Phys. D: Appl. Phys.* **38** 2321
[22] Chen A P, Khatkhatay F, Zhang W, Jacob C, Jiao L and Wang H Y 2013 *J. Appl. Phys.* **114** 124101
[23] Chen B, Gauquelin N, Strkalj N, Huang S, Halisdemir U, Nguyen M D, Jannis D, Sarott M F, Eltes F and Abel S 2022 *Nat. Commun.* **13** 1
[24] Wu X D, Dye R C, Muenchausen R E, Foltyn S R, Maley M, Rollett A D, Garcia A R and Nogar N S 1991 *Appl. Phys. Lett.* **58** 2165

[25] Gao X S, Bao D H, Birajdar B, Habisreuther T, Mattheis R, Schubert M A, Alexe M and Hesse D 2009 *J. Phys. D Appl. Phys.* **42** 175006
[26] James A R and Xi X X 2002 *J. Appl. Phys.* **92** 6149
[27] Nakagawara O, Kobayashi M, Yoshino Y, Katayama Y, Tabata H and Kawai T 1995 *J. Appl. Phys.* **78** 7226
[28] Liu Z X *et al* 2004 *J. Appl. Phys.* **95** 4019
[29] Harrington S A, Zhai J, Denev S, Gopalan V, Wang H, Bi Z, Redfern S A, Baek S-H, Bark C W and Eom C-B 2011 *Nat. Nanotechnol.* **6** 491
[30] Enriquez E, Li Q, Bowlan P, Lu P, Zhang B, Li L, Wang H, Taylor A J, Yarotski D and Prasankumar R P 2020 *Nanoscale* **12** 18193